

Eddy Current Loss Estimation of Edge Burr-Affected Magnetic Laminations Based on Equivalent Electrical Network—Part I: Fundamental Concepts and FEM Modeling

Hamed Hamzehbahmani, Philip Anderson, Jeremy Hall, and David Fox

Abstract—Cutting and punching of the electrical steel can cause edge burrs which lead to interlaminar short circuits between the laminations. In this paper, based on an equivalent electric circuit of the eddy current path, an analytical method has been developed to estimate the eddy current power loss of the magnetic cores, caused by the interlaminar faults, in a wide range of flux density and magnetizing frequency. Important factors, such as skin effect, nonuniform flux density distribution, complex relative permeability, and the nonlinear relation of $B(H)$, which are often neglected in the literature, are highlighted. Fundamental concepts of the interlaminar fault and its consequences, the effect of interlaminar faults on the configuration of magnetic cores, and finite-element method verification are presented in this Part I paper. Modeling of eddy current, together with experimental results of eddy current measurements of packs of shorted laminations, are reported in Part II.

Index Terms—Complex relative permeability, eddy current power loss, edge burr, finite-element method (FEM) modeling, high frequencies, interlaminar fault, skin effect.

I. INTRODUCTION

MAGNETIC cores of electrical machines are constructed from laminations of magnetic steel core material alloyed with silicon to minimize the hysteresis and eddy current losses for high-efficiency operation [1]. Since the magnetic cores are exposed to time-varying magnetic fields, eddy currents are induced in the laminations and consequently, energy is converted into heat in the resistance of the eddy current path. The laminations are coated with insulation material on either side to prevent electrical conduction between the sheets. However, punching and cutting of the electrical steel to the required dimensions can cause edge burrs which are one of the most serious obstacles to precision manufacturing and manufacturing processes automation [2]–[5]. Burrs are formed in various machining process as a result of plastic deformation during mechanical manufacturing processes (e.g., cutting and punching), and have to be removed by a deburring process for functional and technical reasons after the workpiece is machined. The cut

and punch edge shall not exceed 0.05 mm on a length of lamination strip of 10 mm. Punctual edges are allowed up to 0.1 mm [6]. In some designs of electrical machines, high surface insulation resistance is a major requirement and a thick coating is normally used to ensure short circuits arising from burrs are not problematical [7]. However, particular coating or adding a deburring process means extra cost, extra manufacturing time, and an extra machining station [8]. Since burr generation in machining cannot be avoided completely, it is necessary to study their effects and consequences on the magnetic and electrical properties of electrical machines.

Edge burrs could lead to short circuits between adjacent laminations. However, if edge burrs appear between two sheets of the magnetic core on one side only, it does not create a closed current path and no change in the total iron loss of the core occurs. But if the same two sheets are short-circuited on both sides, a closed conductive path will be available which leads to a larger section for the flow of interlaminar eddy currents which results in elevated eddy current loss [9]. Fig. 1(a) shows a 3-D view of a transformer limb with an interlaminar fault in the top step. Eddy current in laminations without fault and interlaminar eddy currents in the presence of the fault, from the cross-sectional view of Fig. 1(a), are shown in Fig. 1(b) and (c), respectively.

A few shorts between the laminations may not create a high interlaminar eddy current; but with several shorts on either side of the core, the induced interlaminar eddy currents could be large and cause excessive local heating in the damaged area [10]. If the generated heat cannot be dissipated adequately, it can cause more interlaminar failures and may eventually cause burning or melting of the iron core and, thus, it raises the potential of a complete machine failure [10]–[17]. Localized heating due to the interlaminar fault currents can also damage the excitation winding insulation and lead to ground failure [1]. Two examples of core melting caused by interlaminar insulation failure are shown in Fig. 2 [1], [10].

In this Part I paper, the fundamental concepts of an interlaminar fault and its consequences on magnetic cores are discussed. The effect of the interlaminar fault on the configuration of laminations and eddy current distribution of the magnetic cores in a wide range of frequencies by focusing on the skin effect are presented. Finally, FEM verification and flux density distribution along the equivalent configuration of magnetic cores with the interlaminar fault are presented.

Manuscript received January 21, 2013; revised April 22, 2013; accepted June 29, 2013. Paper no. TPWRD-00096-2013.

H. Hamzehbahmani, P. Anderson, and J. Hall are with the Wolfson Centre for Magnetics, Cardiff University, Cardiff CF24 3AA, U.K.

D. Fox is with the Cogent Power Ltd., Newport NP19 0RB, U.K.

Color versions of one or more of the figures in this paper are available online at <http://ieeexplore.ieee.org>.

Digital Object Identifier 10.1109/TPWRD.2013.2272663

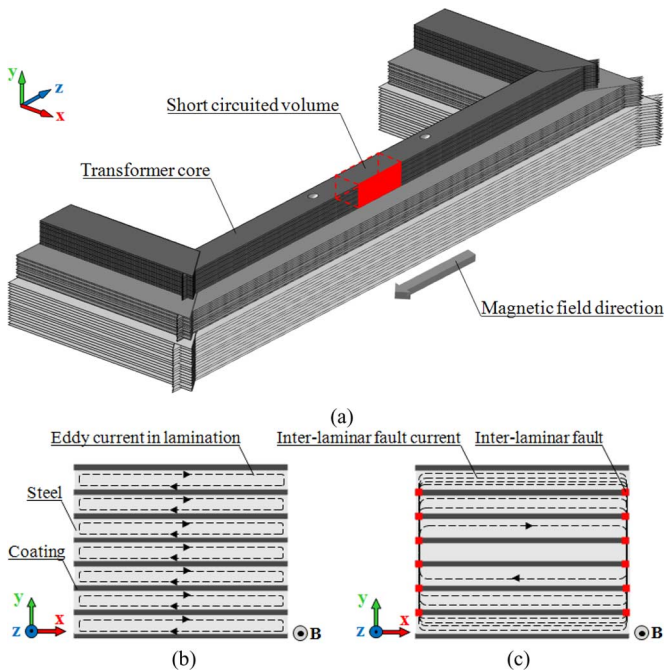


Fig. 1. (a) The 3-D view of a transformer limb with interlaminar short in the top step. (b) Eddy current path in the laminations without the interlaminar fault. (c) Interlaminar eddy current path with interlaminar fault.

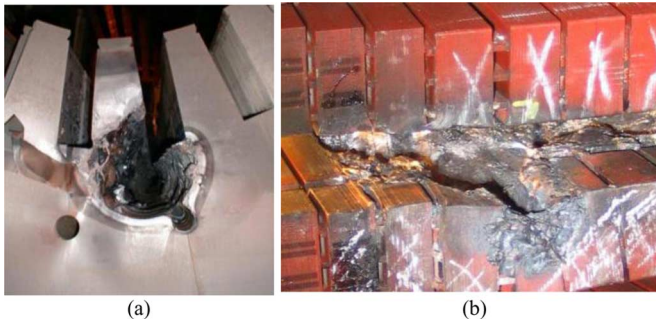


Fig. 2. Stator core melting caused by interlaminar insulation failure. (a) Core fault in tooth wall [1]. (b) Core fault in tooth bottom [10].

II. NATURE OF THE EDDY CURRENT AND EDDY CURRENT POWER LOSS

When a time-varying magnetic field is applied to a conducting material, an electromotive force (emf) is induced in the material, in accordance with Faraday's law of induction. Considering the electrical conductivity of the material, the induced emf along a closed path inside the material sets up a current along that path to circulate and penetrate conducting parts. The direction of the eddy current is perpendicular to the direction of the magnetic field, while the distribution pattern depends on the shape of the conductor. Fig. 3 shows the induced eddy current for cubic and cylindrical-shape conducting materials. Regardless of the driving force, the eddy current density is found to be greatest at the conductor's surface, with a reduced magnitude deeper in the conductor.

That decline in current density is known as the *skin effect* and *depth of penetration* or *skin depth* is a measure of the depth at which the current density falls to e^{-1} (approximately 0.367) of

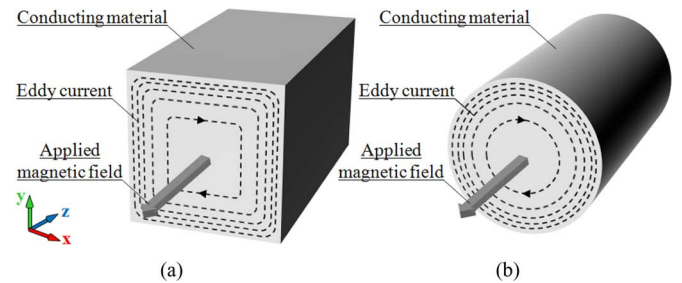


Fig. 3. Induced eddy current in conducting materials exposed to the time-varying magnetic field.

its value near the surface [18]. The skin depth δ of any conducting material is defined by

$$\delta = \sqrt{\frac{2}{\omega\mu\sigma}} = \frac{1}{\sqrt{\pi f\mu\sigma}} \quad (1)$$

where f (Hz), μ (H/m), and σ (S/m) are frequency, absolute magnetic permeability, and electrical conductivity of the material, respectively. From (1), for each material with given permeability and conductivity, the penetration of the eddy current, which is quantified by skin depth, is highly frequency dependent. For conductors with small relative diameter and low operating frequency, the skin effect might be negligible. However, at higher frequencies, where the skin depth is smaller, the effective cross-section is reduced and, hence, the effective resistance of the conductor is increased and it affects the characteristics of the conductor. Therefore, skin depth is a determinant parameter in eddy current modeling and estimation, especially at high frequencies.

Eddy currents and, hence, eddy current power loss are minimized in the magnetic devices by using thin sheets of magnetic material, known as laminations. Laminating the magnetic cores can reduce the skin effect at low frequencies as well. At high frequencies, the skin effect is an important factor and should be taken into account in accurate modeling of the eddy current loss. However, in a burr-affected magnetic core, the skin effect might become significant even at low frequencies.

III. FLUX DENSITY DISTRIBUTION INSIDE SINGLE-SHEET MAGNETIC LAMINATION

One of the major factors in eddy current power loss determination is the magnetic flux density distribution along the thickness of the lamination which depends on magnetizing frequency. Fig. 4 shows a 3-D view of a single sheet lamination of thickness $t = 2a$ in a time-varying magnetic field $B_s \cos\omega t$ (B_s : flux density at surface) applied in the rolling direction.

In this figure, the z and y directions represent rolling and transverse (90° to the direction of rolling) directions of the lamination, respectively. If eddy current loops are assumed to be large enough along the transverse direction, the field problem becomes 1-D and can be reduced to a single equation for the z -component of magnetic flux density $B_z(x, t)$ that depends on x and t [19]

$$\frac{\partial^2 B_z(x, t)}{\partial x^2} = \mu_0\mu_z\sigma \frac{\partial B_z(x, t)}{\partial t} \quad (2)$$

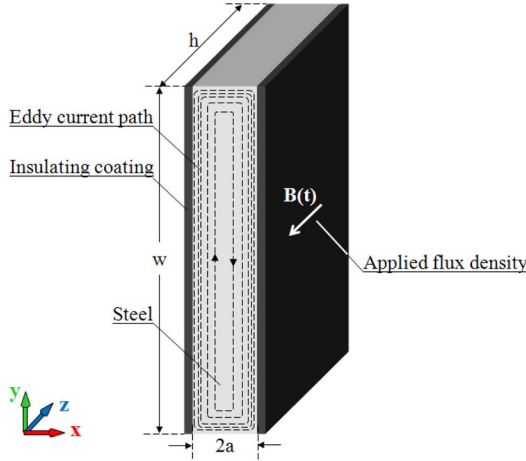


Fig. 4. The 3-D view of a magnetic lamination of thickness $2a$ under the time-varying magnetic field $\mathbf{B}(t)$.

where μ_z is the permeability of the material at a particular flux density B_z . Equation (2) is a differential equation which defines the flux density B_z as a function of distance x and time t and has the value $B_s \cos \omega t$ when x is $\pm a$. This equation was solved for particular relative permeability and magnetic flux density based on the method stated in [19]; therefore, the instantaneous flux density at any point inside the lamination is obtained by

$$B_z(x, t) = B_s \sqrt{\frac{\cosh \frac{2x}{\delta} + \cos \frac{2x}{\delta}}{\cosh \frac{2a}{\delta} + \cos \frac{2a}{\delta}}} \cos(\omega t - \beta) \quad (3)$$

where δ is skin depth, which was defined by (1), and β is the phase angle of the flux density and can be obtained by (4), shown at the bottom of the page, where $p = 1/\delta$. Equation (3) defines flux density along the thickness of the lamination as a function of distance x from the center line of the lamination, skin depth δ , and time t . Substituting $x = \pm a$ into (3), the flux density at the surface of the lamination is obtained as

$$B_z(a, t) = B_z(-a, t) = B_s \cos \omega t. \quad (5)$$

A. Flux Density Dependence of the Relative Permeability

In order to extend the solution of (2) to a wide range of flux density, the nonlinear relation of $B(H)$ was taken into account by measuring the relative permeability of the material. Neglecting flux leakage around the magnetic core, effective relative permeability μ_r as a function of magnetic flux density can be obtained using the following equation [20]:

$$\mu_r = \frac{B_{pk} l_m}{\mu_0 N I_{pk}} \quad (6)$$

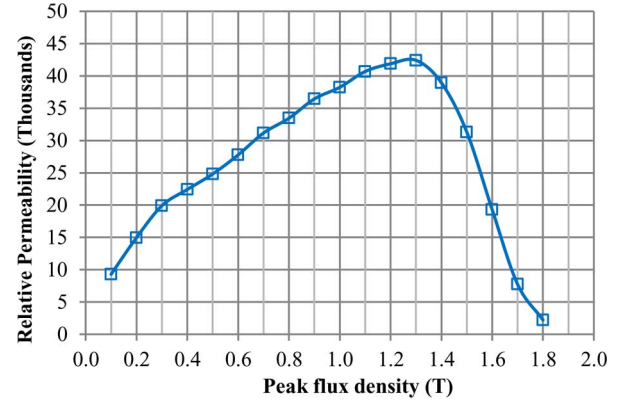


Fig. 5. Flux density dependence of the effective relative permeability of CGO at the magnetizing frequency of 50 Hz.

where B_{pk} is peak values of magnetic flux density, l_m is the mean magnetic path length of the magnetic circuit, μ_0 is the permeability of free space, N is the number of turns of the magnetizing coil, and I_{pk} is the measured peak magnetizing current. Based on (6), the relative permeability of a single sheet lamination of CGO at flux densities 0.1 to 1.8 T and 50-Hz frequency was measured using a single-sheet tester (SST); the result is shown in Fig. 5. As shown in this figure, the relative permeability of the magnetic laminations varies significantly with flux density. To increase the accuracy of the analytical model, this variation should be considered in calculating eddy current power loss and other magnetic quantities.

B. Complex Relative Permeability at High Frequencies

Due to the inductive nature of the magnetic materials, there is a time lag between magnetic flux density \mathbf{B} and magnetic-field strength \mathbf{H} . However, at low frequencies, this time lag is negligible but at high frequencies, it might be significant and should be taken into account. To analyze these phenomena in magnetic cores, it is convenient to consider the relative magnetic permeability of the material as the complex quantity $\mu_r = \mu'_r - j\mu''_r$ in which μ'_r and μ''_r are real functions of the magnetizing frequency f [21]. The effective relative complex permeability of the lamination in the rolling direction can be obtained by [21]

$$\mu_z^{\text{eff}} = \mu'_z - j\mu''_z = \mu_z \frac{\tanh(a\gamma)}{a\gamma} \quad (7)$$

where μ_z is the absolute static permeability of the material in the rolling direction and γ is the propagation constant which is directly related to the skin depth δ by [21]

$$\gamma = \frac{(1+j)}{2\delta}. \quad (8)$$

Real and imaginary parts of the effective complex permeability as a function of the magnetizing frequency are shown

$$\tan \beta = \frac{\sinh p(a-x) \sin p(a+x) + \sinh p(a+x) \sin p(a-x)}{\cosh p(a-x) \cos p(a+x) + \cosh p(a+x) \cos p(a-x)} \quad (4)$$

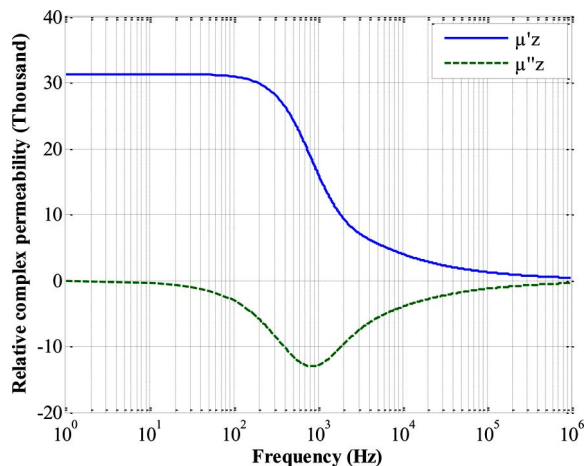


Fig. 6. Real and imaginary parts of the relative complex permeability of a single-strip magnetic lamination in the rolling direction at a peak flux density of 1.5 T.

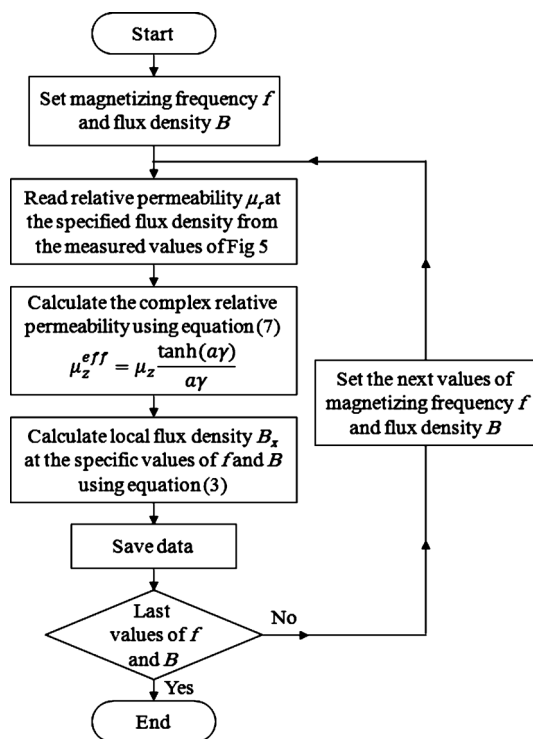


Fig. 7. Flowchart of calculation of the flux density distribution.

in Fig. 6. The computations of Fig. 6 were performed using the following parameters for 3% grain-oriented silicon steel material: thickness = 0.3 mm, conductivity, $\sigma = 2.17 \times 10^6$ S/m (measured based on the method in [22]) relative permeability, $\mu_z = 3.13 \times 10^4$ at a peak flux density of 1.5 T (derived from Fig. 5).

A flowchart was designed to calculate the magnetic flux density distribution along the lamination thickness at each frequency and flux density, as shown in Fig. 7. According to the designed flowchart, the magnetizing frequency and amplitude of the flux density are initially set at the required values. Relative permeability μ_r at the specific flux density is then read from the measured values of Fig. 5. Complex relative

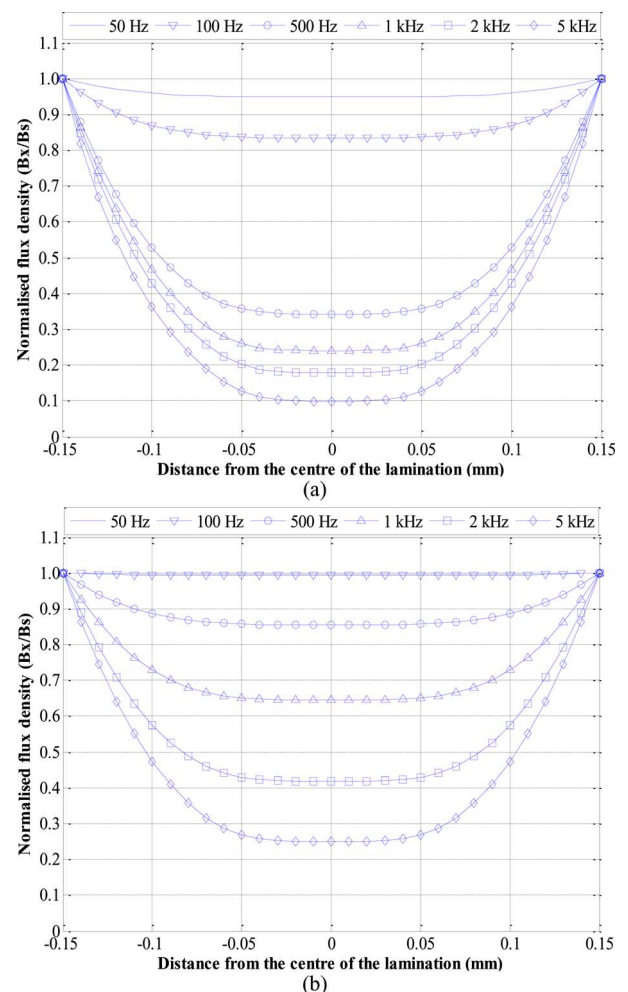


Fig. 8. Normalized magnetic flux density penetration into the magnetic lamination of thickness $2a = 0.3$ mm at different frequencies. (a) $B_s = 1.3$ T. (b) $B_s = 1.7$ T.

permeability of the material will then be calculated using (7); and, finally, local flux density B_x at the specific values of magnetizing frequency and the amplitude of surface flux density will be calculated using (3).

Based on the design flowchart, magnetic flux density distribution (normalized by the value at the surface) along the thickness of the lamination for different values of the magnetizing frequency f and particular surface flux densities 1.3 T and 1.7 T are shown in Fig. 8. These curves were obtained by the following parameter values for 3% GO silicon steel with a thickness of 0.3 mm: $\sigma = 2.17 \times 10^6$ S/m and $\mu_r = 4.24 \times 10^4$ at 1.3 T and $\mu_r = 7.75 \times 10^3$ at 1.7 T.

Two important notes could be taken from Fig. 8. The first note is related to flux density distribution along the lamination thickness. From (3), half of the lamination thickness a and skin depth δ are two determinant factors in the qualification of the flux density distribution along the lamination thickness. At low frequencies, where $\delta \gg a$, flux density distributes uniformly along the lamination thickness. However, at high frequencies where $\delta \ll a$, the flux density at the center region of the lamination is nearly zero, and corresponding high flux density is noted near the surfaces of the lamination. And, second, Fig. 8

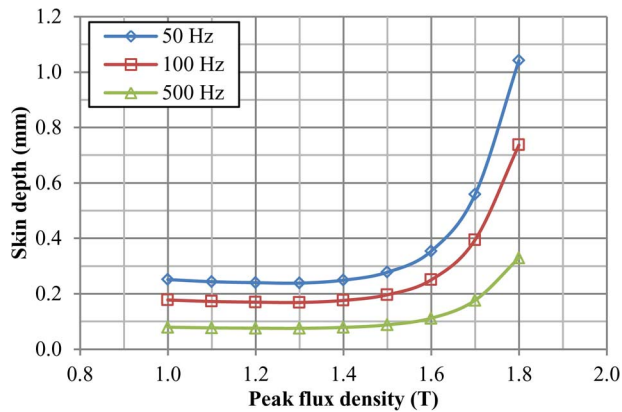


Fig. 9. Effect of flux density on skin depth for CGO material at magnetizing frequencies 50, 100, and 500 Hz.

shows that flux density distribution along the lamination thickness not only depends on magnetizing frequency but also depends on peak magnetic flux density which is related to the non-linear relation of $B(H)$.

From (1), at a specific frequency, the only parameter that could vary with flux density is the relative permeability of the material which, in turn, could affect the flux density penetration. In order to investigate this phenomenon, variation of the skin depth of CGO material was calculated at magnetizing frequencies of 50, 100, and 500 Hz and flux density from 1.0 to 1.8 T. The results are shown in Fig. 9. This figure shows significant skin effect at low flux densities; however, this effect becomes negligible at high flux densities. These fluctuations are related to the effect of flux density on the relative permeability or non-linear relation of $B(H)$.

IV. EFFECT OF INTERLAMINAR FAULT ON THE CONFIGURATION OF THE MAGNETIC CORES

In a perfectly assembled core, when the laminations are well insulated from each other, the eddy current paths are restricted to individual laminations, as shown in Fig. 1(b). This is due to the insulation coating on the surface of the steel preventing the electrical connection between adjacent laminations [5]. The primary hypothesis about the effect of the edge burr on the magnetic cores is to change the configuration of the burred laminations to a solid core with an equivalent thickness of $2na$, where n is number of the adjacent burred laminations and a is half of the thickness of one lamination. This hypothesis for packs of two and three laminations is illustrated in Fig. 10.

A. FEM Verification

In order to verify this hypothesis, 2-D FEM simulations for stacks of two, three, and five laminates were performed using COMSOL Multiphysics. Fig. 11 shows the FEM mesh model for the upper end above the line of symmetry of a stack of five laminations with interlaminar short. Each lamination has a thickness of 0.3 mm and they are separated by an air gap of 20 μm . The laminations were exposed to a time-varying outward magnetic field (perpendicular to the page). As the first part of this investigation, the laminations were magnetized without the interlaminar fault and with the interlaminar fault on one side

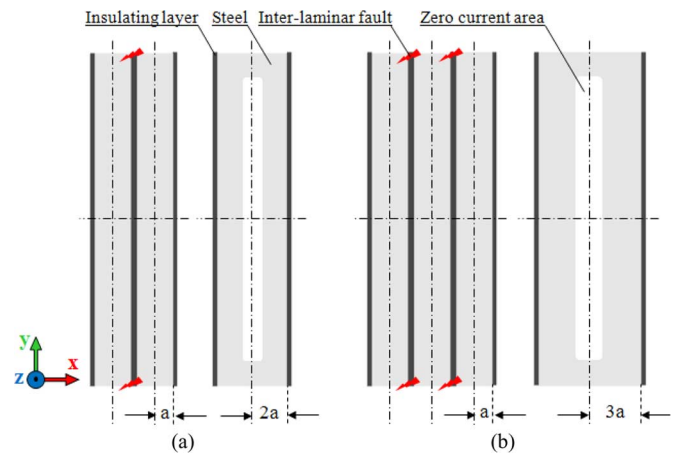


Fig. 10. Cross-sectional area of (a) two and (b) three magnetic laminations of thickness $2a$ with a short circuit on either side and equivalent configurations.

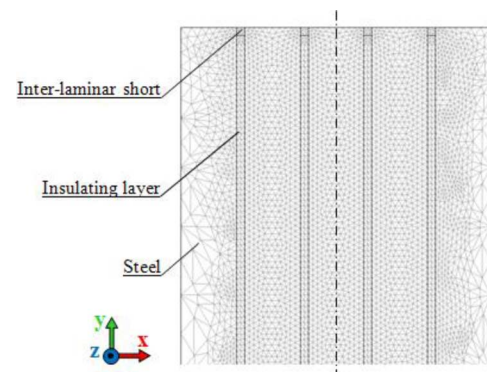


Fig. 11. FEM mesh model of five laminations with an interlaminar short circuit.

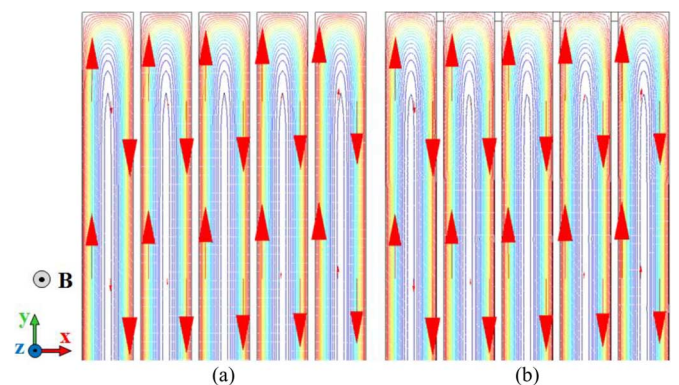


Fig. 12. Eddy current distribution in a stack of five laminations (a) without the interlaminar fault and (b) with the interlaminar fault on one side only; at 50 Hz.

only. The result of this investigation at the magnetizing frequency of 50 Hz is shown in Figs. 12(a) and (b), respectively.

Fig. 12(a) shows the ideal performance of magnetic cores, that is, without the interlaminar fault between the laminations, in which eddy currents are restricted to individual laminations. On the other hand, as expected initially, eddy currents at the shortened end of Fig. 12(b) are still restricted to the individual laminations. Interlaminar eddy current between the laminations requires a closed path perpendicular to the flux density in the core. Therefore, as shown in Fig. 12(b), if edge burrs appear

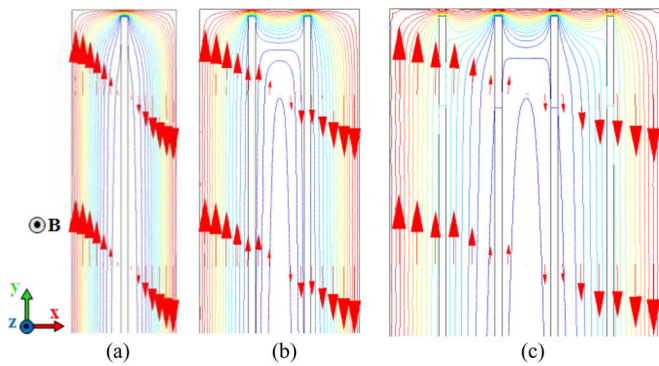


Fig. 13. The 2-D FEM modeling of eddy current distribution in burred magnetic laminations at a magnetizing frequency of 50 Hz: (a) two, (b) three, and (c) five laminations.

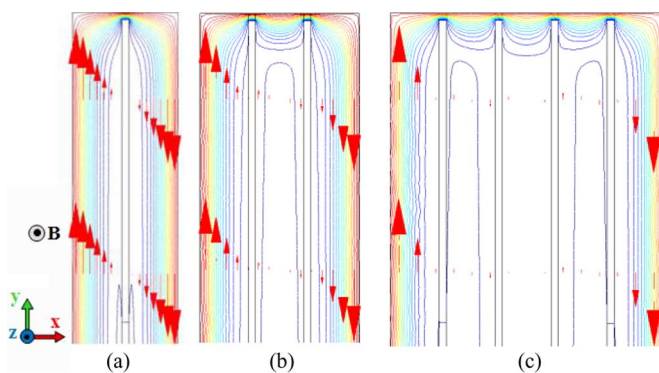


Fig. 14. The 2-D FEM modeling of eddy current distribution in burred magnetic laminations at a magnetizing frequency of 1000 Hz: (a) two, (b) three, and (c) five laminations.

between the laminations of the magnetic core on one side only, it does not create a closed current path and no change in the eddy current distribution and, hence, eddy current power loss occurs.

Magnetic laminations were then shorted together on either side. Eddy current distribution in the cores with two, three, and five laminations with the interlaminar fault on both sides at magnetizing frequencies of 50 and 1000 Hz are shown in Figs. 13 and 14, respectively. Due to the known symmetry in the y -direction, only one end of the laminations is shown.

Five important points could be concluded from the FEM results of Figs. 12 and 13 as follows.

- 1) There is only one eddy current loop in each pack of the shorted laminations, which can prove the primary hypothesis.
- 2) The interlaminar faults change the configuration of the magnetic cores to be similar to a solid core which leads to interlaminar fault current and larger eddy current loops.
- 3) Eddy current density at the shorted ends is much higher than the laminations which lead to local power loss at the shorted ends.
- 4) Changing the configuration of the burred laminations causes the skin effect to become significant, even at low frequencies.
- 5) The equivalent configuration, which is affected by the skin effect, leads to a zero current area at the center line of the equivalent configuration. The position and width of the

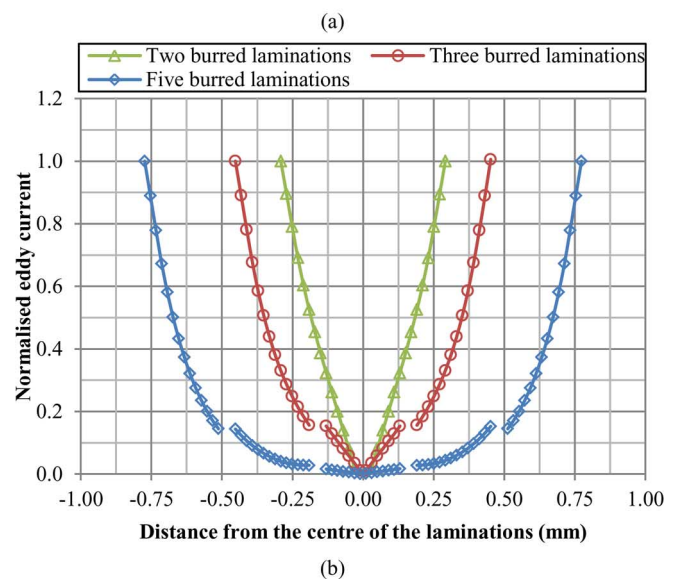
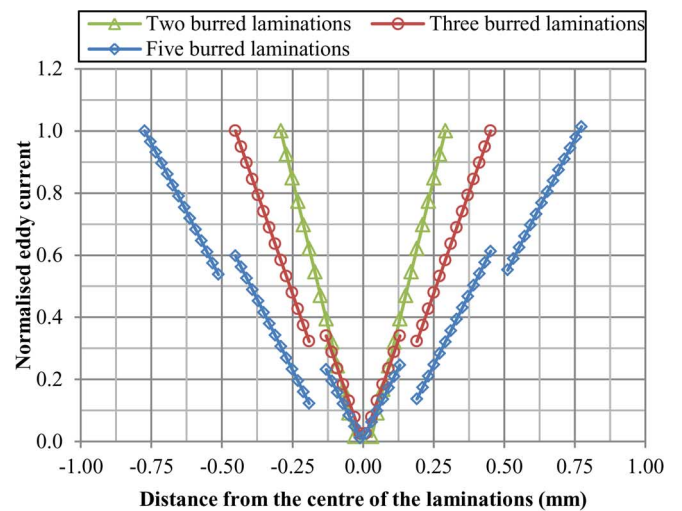


Fig. 15. FEM result of normalized induced eddy current density in packs of two, three, and five laminations at frequencies (a) 50 Hz and (b) 1000 Hz.

zero current area in the equivalent configurations depends on the number of the shorted laminations, magnetizing frequency, and flux density.

In order to visualize eddy current distribution along the shorted laminations, the FEM results of induced eddy current density normalized by the surface value for packs of two, three, and five shorted laminations at magnetizing frequencies of 50 Hz and 1000 Hz are shown in Fig. 15(a) and (b), respectively.

Fig. 15 shows that regardless of the gaps between the shorted laminations, the induced eddy currents in the laminations at 50 Hz are a linear function of distance from the center line, but not at 1000 Hz. It will be discussed further in Section 2.1 of the Part II paper based on the induced voltage in the magnetized lamination. However, these curves emphasize the importance of skin effect on magnetic properties of burred laminations. Therefore, to investigate the effect of interlaminar fault on the magnetic properties of the magnetic cores, shorted laminations can be modeled by a solid core with an equivalent thickness of $2na$. However, as demonstrated by FEM modeling, in the presence of the interlaminar fault, the skin effect becomes significant, even

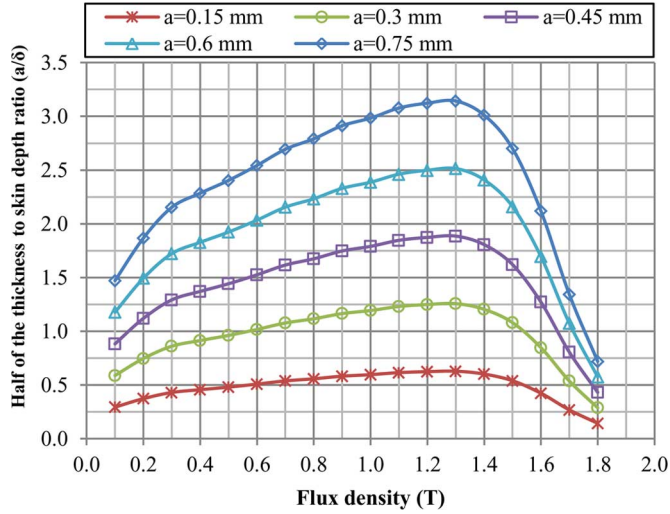


Fig. 16. Half of the thickness to skin depth ratio (a/δ) versus flux density at different thicknesses at 50-Hz frequency.

at low frequencies, and should be taken into account in the related studies.

B. Flux Density Distribution in Burred Laminations

From (3), half of the lamination thickness a and skin depth δ are two determinant factors in the qualification of the flux density distribution along the lamination thickness. In time-harmonic investigations, it is usual to compare the thickness or diameter of the cross section of the conducting materials with the equivalent skin depth at each particular operating point. Therefore, it is useful to compare the ratio of half of the lamination thickness to the skin depth (a/δ) for different thicknesses, flux densities, and magnetizing frequencies. Fig. 16 shows the a/δ ratio versus flux density for different lamination thicknesses at a magnetizing frequency of 50 Hz. The curves of $a = 0.15$ mm indicate a/δ ratio versus flux density of the single-strip lamination and the curves of $a = 0.3$ mm, $a = 0.45$ mm, $a = 0.6$ mm, and $a = 0.75$ mm are equal to those of the packs of two, three, four, and five shorted laminations, respectively.

Fig. 16 shows that for a single lamination with $a = 0.15$ mm (thickness of 0.3 mm) at 50-Hz frequency, $a/\delta < 1$ for all flux densities. Therefore, in this case, the skin effect can be neglected and flux density distributes almost uniformly along the lamination thickness, as shown in Fig. 8. However, since skin depth δ is a constant value at a given frequency and flux density, by increasing the thickness of the lamination, it will become significant (i.e., the a/δ ratio becomes greater than unity even at low frequency). Therefore, considering the effect of the edge burrs on the configuration of the burred laminations, significant skin effect and nonuniform flux density distribution along the equivalent thickness of the burred laminations are expected, even at low frequencies.

From (7) and (8), the skin effect δ and half of the lamination thickness a are also two key factors in complex relative permeability. Therefore, interlaminar short circuits also affect the complex relative permeability of the material. Amplitude and

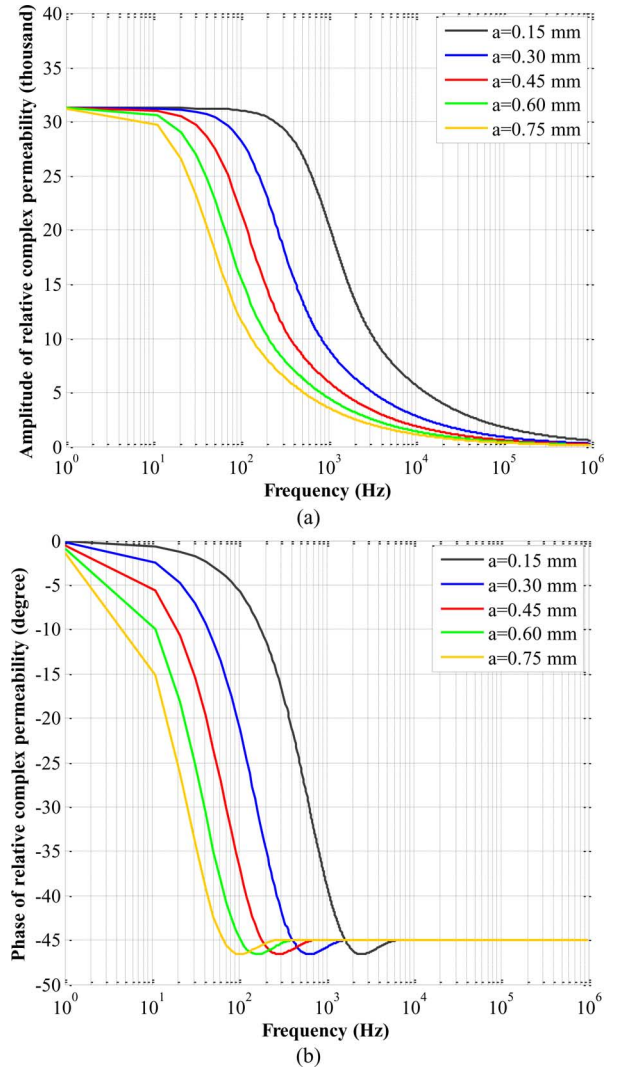


Fig. 17. Frequency dependence of (a) amplitude and (b) phase of the relative complex permeability of a magnetic lamination in the rolling direction for different lamination thicknesses at $B_s = 1.5$ T.

phase angle of the complex relative permeability of the material with the specifications given in Section III typically at surface flux density $B_s = 1.5$ T for five different thicknesses, $a = 0.15$ to $a = 0.75$ mm are shown in Fig. 17. The amplitude of the complex relative permeability decreases by increasing the magnetizing frequency. However, in the presence of interlaminar faults, which lead to an increase of the effective thickness of the damaged laminations, the amplitude of the complex relative permeability is reduced at lower frequencies, that is, for laminations of 0.3-mm thickness, complex relative permeability is constant up to about 100 Hz while for the lamination of 1.5-mm thickness, it drops at a few Hertz. Therefore, in the presence of the interlaminar fault, the complex relative permeability becomes more significant and should be taken into account, even at low frequencies.

Using the designed flowchart of Fig. 7, normalized flux density distributions along the lamination thickness at surface flux densities 1.3 T and 1.7 T and the magnetizing frequency of 50 Hz for different thicknesses of the lamination from 0.3 to 1.5

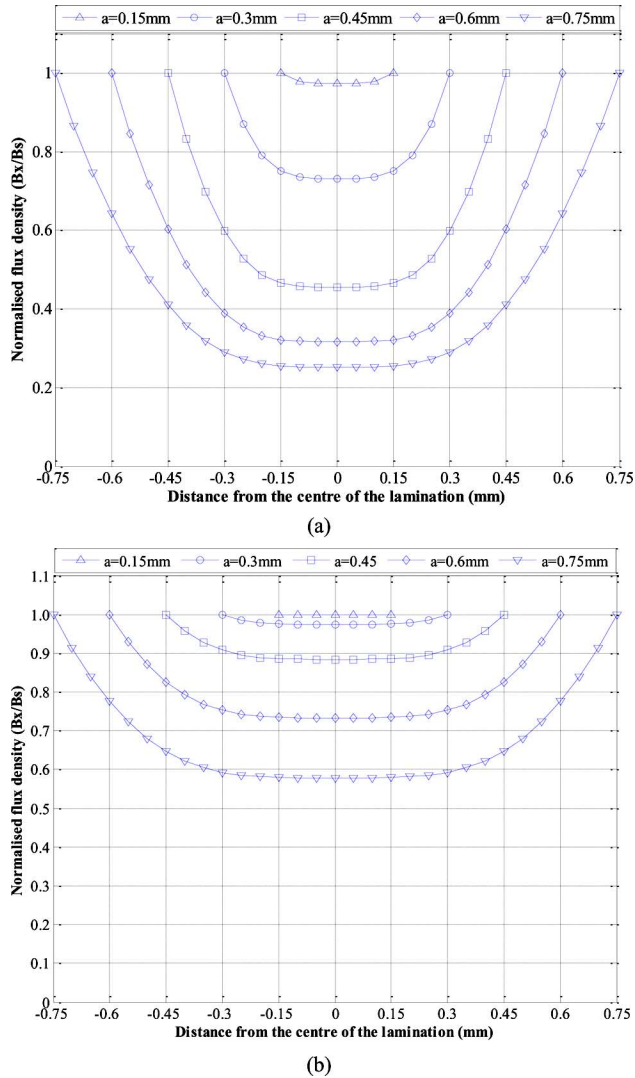


Fig. 18. Normalized flux density penetration into the lamination of different thicknesses at a frequency of 50 Hz and surface flux density (a) $B_s = 1.3$ T and (b) $B_s = 1.7$ T.

mm are shown in Fig. 18. In these curves, the nonlinear relation of $B(H)$ and complex relative permeability of Fig. 17 were taken into account. The results presented in Fig. 18 show that at 50 Hz, flux density is distributed almost uniformly along the lamination with a thickness of 0.3 mm; however, by increasing the lamination thickness, at the same flux density and magnetizing frequency, half of the thickness a will become greater than the skin depth δ and, therefore, the flux density drops from the edge of lamination to the center line.

Therefore, it can be concluded that the importance of the skin effect on the eddy current distribution and eddy current power loss is not only at high frequencies, but also at low frequencies when the core is affected by interlaminar faults.

V. CONCLUSION

In this Part I paper, fundamental concepts of the interlaminar fault and its consequences on the magnetic cores were presented. An equivalent configuration was proposed for magnetic

cores with interlaminar faults. 2-D FEM modeling was performed to verify the equivalent configuration and visualize eddy current paths along the lamination thickness.

Based on FEM modeling and analytical results, it was found that the skin effect is a key factor in the eddy current power-loss investigation of magnetic cores not only at high frequencies, but also at low frequencies when the core is affected by the edge burrs. The proposed configuration in this Part I paper will be used in the Part II paper to estimate eddy current power loss of burr-affected magnetic cores in a wide range of magnetizing frequency and flux density.

ACKNOWLEDGMENT

The authors would like to thank Cogent Power Ltd. for providing the electrical steel sheets.

REFERENCES

- [1] K. Lee, J. Hong, K. Lee, S. B. Lee, and E. J. Wiedenbrug, "A stator core quality assessment technique for inverter-fed induction machines," in *Proc. IEEE Ind. Appl. Soc. Annu. Meeting*, Oct. 2008, pp. 1–8.
- [2] M. B. Aimoniotis and A. J. Moses, "Evaluation of induced eddy currents in transformer sheets due to edge-burrs, employing computer aided design programs," in *Proc. Athens Power Tech*, 1993, vol. 2, pp. 847–849.
- [3] H. Hamzehbahmani, A. J. Moses, and F. J. Anayi, "Opportunities and precautions in measurement of power loss in electrical steel laminations using the initial rate of rise of temperature method," *IEEE Trans. Magn.*, vol. 49, no. 3, pp. 1264–1273, Mar. 2013.
- [4] A. J. Moses and M. Aimoniotis, "Effects of artificial edge burrs on the properties of a model transformer core," *Phys. Scripta*, vol. 39, pp. 391–393, 1989.
- [5] R. Mazurek, P. Marketos, A. J. Moses, and J. N. Vincent, "Effect of artificial burrs on the total power loss of a three-phase transformer core," *IEEE Trans. Magn.*, vol. 46, no. 2, pp. 638–641, Feb. 2010.
- [6] *Laminations for Transformers and Inductors—Part I: Mechanical and Electrical Characteristics*, BS EN 60740-1:2005, 2005.
- [7] M. Lindenmo, A. Coombs, and D. Snell, "Advantages, properties and types of coatings on non-oriented electrical steels," *J. Magn. Mater.*, vol. 215–216, pp. 79–82, 2000.
- [8] W. J. Deng, Z. C. Xie, P. L. , and T. K. Xu, "Study on burr formation at the top edge in rectangular groove cutting," *J. Advances Mater. Sci. Eng.*, vol. 2012.
- [9] C. A. Schulz, S. P. Duchesne, D. Roger, and J. N. Vincent, "Capacitive short circuit detection in transformer core laminations," *J. Magn. Mater.*, vol. 320, pp. e911–e914, 2008.
- [10] D. B. Paley, "Current low power core testing using EL CID," *IEEE Colloq. "Understanding Your Condition Monitoring (Ref. No. 1999/117)"*, pp. 7/1–7/4, Apr. 1999.
- [11] D. R. Bertenshaw, J. F. Lau, and D. J. Conley, "Evaluation of EL CID indications not associated with stator core inter-laminar insulation faults," in *Proc. IEEE Elect. Insul. Conf.*, Jun. 2011, pp. 254–260.
- [12] D. B. Paley, "Current low power core testing using EL CID," *IEEE Colloq. "Understanding Your Condition Monitoring (Ref. No. 1999/117)"*, pp. 7/1–7/4, Apr. 1999.
- [13] C. A. Schulz, S. Duchesne, D. Roger, and J. N. Vincent, "Short circuit current measurements between transformer sheets," *IEEE Trans. Magn.*, vol. 46, no. 2, pp. 536–539, Feb. 2010.
- [14] C. A. Schulz, D. Roger, S. Duchesne, and J. N. Vincent, "Experimental characterization of interlamination shorts in transformer cores," *IEEE Trans. Magn.*, vol. 46, no. 2, pp. 614–617, Feb. 2010.
- [15] S. B. Lee, G. Kliman, M. Shah, D. Kim, T. Mall, K. Nair, and M. Lusted, "Experimental study of inter-laminar core fault detection techniques based on low flux core excitation," *IEEE Trans. Energy Convers.*, vol. 21, no. 1, pp. 85–94, Mar. 2006.
- [16] S. B. Lee, G. B. Kliman, M. R. Shah, N. K. Nair, and R. M. Lusted, "An iron core probe based inter-laminar core fault detection technique for generator stator cores," *IEEE Trans. Energy Convers.*, vol. 20, no. 2, pp. 344–351, Jun. 2005.
- [17] S. B. Lee, G. B. Kliman, M. R. Shah, W. T. Mall, N. K. Nair, and R. M. Lusted, "An advanced technique for detecting inter-laminar stator core faults in large electric machines," *IEEE Trans. Ind. Appl.*, vol. 41, no. 5, pp. 1185–1193, Sep./Oct. 2005.

- [18] Z. Popovic and B. D. Popovic, *Introductory Electromagnetics*. Upper Saddle River, NJ: Prentice-Hall, 2000.
- [19] F. Brailsford, *Physical Principles of Magnetism*. New York: Van Nostrand, 1966.
- [20] M. B. Balehosur, Ph. Marketos, A. J. Moses, and J. N. Vincent, "Packet-to-packet variation of flux density in a three-phase, three-limb power transformer core," *IEEE Trans Magn.*, vol. 46, no. 2, pp. 642–645, Feb. 2010.
- [21] K. G. Nilanga, B. Abeywickrama, T. Daszczyński, Y. V. Serdyuk, and S. M. Gubanski, "Determination of complex permeability of silicon steel for use in high-frequency modeling of power transformers," *IEEE Trans Magn.*, vol. 44, no. 4, pp. 438–444, Apr. 2008.
- [22] P. Anderson, D. R. Jones, and J. Hall, "Measurement of resistivity of soft magnetic laminations at elevated temperatures," *J. Magn. Mater.*, vol. 304, no. 2, pp. e546–e548, 2006.



Hamed Hamzehbahmani was born in Sanandaj, Iran, in 1978. He received the B.Sc. degree in electrical engineering from Birjand University, Birjand, Iran, in 2005, the M.Sc. degree in electrical engineering from Iran University of Science and Technology (IUST), Tehran, Iran, in 2007, and is currently pursuing the Ph.D. degree in electrical engineering from Cardiff University, Cardiff, U.K.

From 2005 to 2008, he was a Supervisor Engineer with Moshanir Power Engineering Consultant, Tehran. He joined the School of Engineering, Azad

University of Sanandaj, as a member of the academic staff. His research interests include eddy current power-loss modeling in electrical steels and interlaminar fault detection in magnetic cores.



Philip Anderson was born in Wales, U.K., in 1972. He received the B.Eng., M.Sc., and Ph.D. degrees from Cardiff University, Cardiff, U.K.

He then joined the European Electrical Steels, Newport, U.K. and has worked at the Wolfson Centre, Cardiff University, since 2000, as a Researcher and then Lecturer in Magnetic Engineering.

Dr. Anderson is a Chartered Engineer and active member of the national and international committees on magnetic steels and alloys.



Jeremy Hall was born in Birmingham, U.K., in 1969. He received the B.Sc. degree from the University of Wales (UC Swansea) in 1992, the M.Sc. degree from Loughborough University, Loughborough, U.K., in 1993, and the Ph.D. degree from Cardiff University, Cardiff, U.K., in 2001.

After receiving the M.Sc. degree, he had a research post in the electrical steels industry in south Wales with European Electrical Steels Ltd. He has been involved in commercial/academic research and, later, had academic appointments with the Wolfson

Centre for Magnetics, Cardiff University. He is a Chartered Physicist and Chief Technical Officer for the university spin-out company, Faultcurrent Ltd.



David Fox was born in England in 1947. He received the B.Eng. (Hons.) degree in electrical and electronic engineering from the University of Bradford and a degree in mathematics from The Open University.

After leaving The Open University, he worked for several years in the development of medical electronics before moving into magnetics with Telmag Magnetic Components and later with Cogent Power Ltd.

Mr. Fox is a Chartered Engineer and Fellow of the Institute of Engineering and Technology.